Supporting Information

Synthesis of metal nitride and metal oxide nanoparticles by atmospheric-pressure spark ablation

Klito C. Petallidou[1*], Dimitris Gounaris[1], Pau Ternero[2], Maria E. Messing[2,3],

Andreas Schmidt-Ott[1,4,5], George Biskos[1,6*]

[1]Climate and Atmosphere Research Centre, The Cyprus Institute, 2121 Nicosia, Cyprus

[2]Department of Physics and NanoLund, Lund University, 22100 Lund, Sweden

[3]Department of Microtechnology and Nanoscience, Chalmers University of Technology, 412 96 Gothenburg, Sweden

[4]Faculty of Applied Sciences, Delft University of Technology, 2629 HZ Delft, The Netherlands

[5]VSPARTICLE B.V, 2629 JD Delft, The Netherlands

[6]Faculty of Civil Engineering and Geosciences, Delft University of Technology, 2628 CN Delft, The Netherlands

Corresponding email addresses

Klito C. Petallidou: k.petallidou@cyi.ac.cy

George Biskos: g.biskos@cyi.ac.cy; g.biskos@tudelft.nl

S.1 Atmospheric-Pressure Spark Ablation

As illustrated in Figure S1, atmospheric-pressure spark ablation produces nanoparticles by repeatedly creating electrical discharges (sparks) between two conductive electrodes. The process relies on the formation of plasma that locally heats and evaporates tiny amounts of material from the electrode surfaces. As the resulting vapors rapidly cool by the carrier gas (e.g., N_2 as used in all our measurements here), they nucleate to form atomic cluster that grow to singlet nanoparticles by further condensation and a agglomerates by coagulation. Spark ablation enables clean, reproducible synthesis of particles whose composition is based on that of the electrodes, ranging from identical matches (e.g., pure metal nanoparticles) to versatile mixtures resulting from the interaction with species in the carrier gas; e.g., nitrogen and oxygen as demonstrated in the main manuscript of this work.

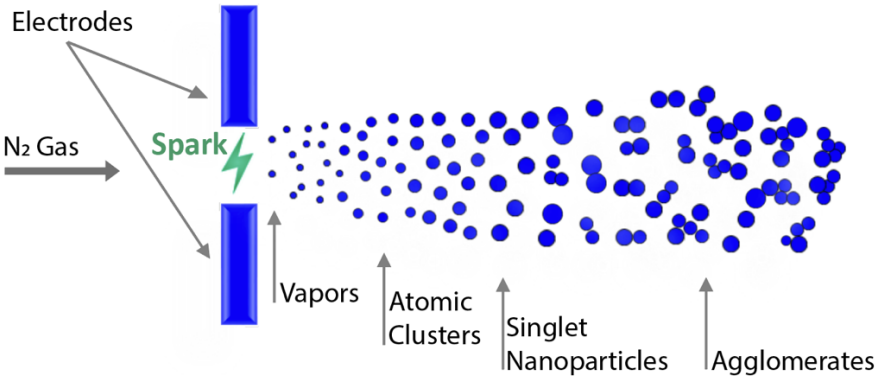

Figure S1. Schematic illustration of the atmospheric-pressure spark ablation process.

S.2 Splashing Particles

Splashing particles (i.e., particles larger than ~100 nm) resulting by spark ablation are produced by the ejection of droplets from locally formed molten pools formed on the surface of the electrodes. Their production depends on the geometry of the electrodes and the properties of the material they are made of (i.e., heat conductivity and melting point). Figure S2 shows a Scanning Electron Microscopy (SEM) image of a splashing particle produced by the spark discharge generator (SDG) we employed in this work using Ti electrodes and N2 as a carrier gas.

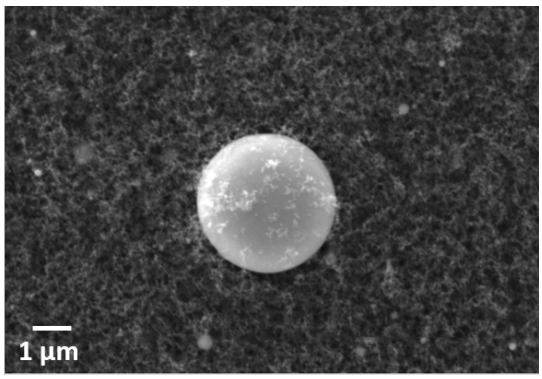

Figure S2. SEM image of a splashing particles produced by the SDG when using Ti electrodes under a N_2 flow.

S.3 Additional X-ray diffraction Measurements

To further evaluate the universality of spark ablation synthesis for metal nitride and oxide nanoparticles, we extended the investigation to Hafnium (Hf), Vanadium (V) and Manganese (Mn). The corresponding X-ray diffraction measurements are provided in Figure S3. Consistent with the results observed for Aluminum and Titanium described in the main manuscript, these highly reactive metals yielded a mixture of nitride and oxide phases. Specifically, the Hf NPs (Figure S3a) exhibits dominant cubic nitride HfN reflections alongside tetragonal HfO_2. The V NPs (Figure S3b) comprise crystalline cubic VN accompanied by a broad low-angle feature characteristic of an amorphous VO_2. Similarly, the Mn NPs (Figure S3c) display a distinct bimodal phase distribution, where cubic Mn_4N coexists with thermodynamically stable, highly crystalline MnO. These findings corroborate the general trend that unless strict oxygen-free conditions are maintained, spark ablation of oxophilic transition metals typically results in nanoparticles containing both nitride and oxide phases.

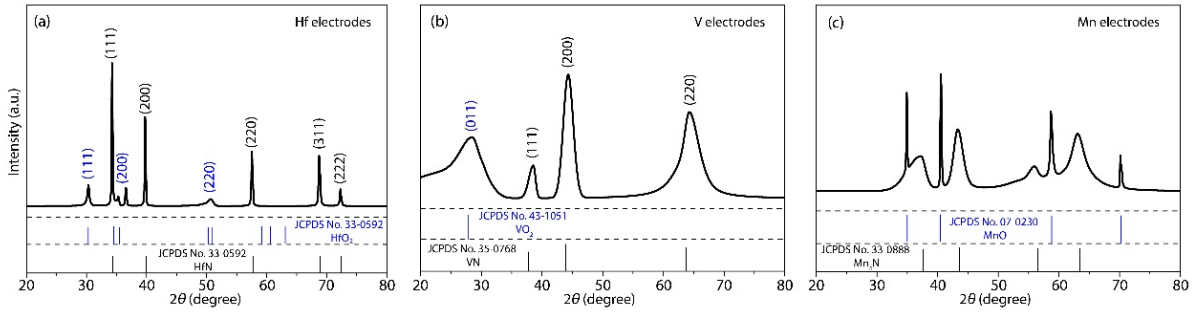

Figure S3. XRD measurements of nanoparticles synthesized by spark ablation using (a) Hf, (b) V, and (c) Mn electrodes. Hf-based particles show dominant cubic HfN reflections alongside HfO_2; V-based particles consist of crystalline cubic VN and monoclinic VO_2; Mn-based particles exhibit a bimodal mixture of highly crystalline cubic MnO and Mn_4N.

S.4 Images of the Filter used to Collect Mg-based Nanoparticles

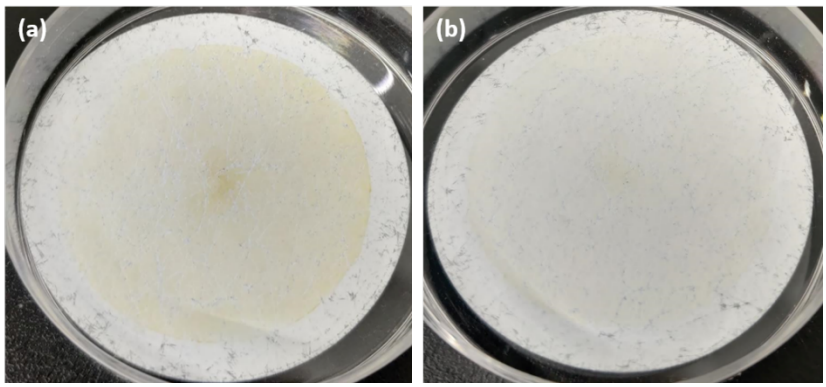

Figure S4. Pictures of the filter of the as-deposited Mg-based nanoparticles (a) immediately after their synthesis, and (b) after exposure to ambient air for a few hours.

S.5 Tabulated Enthalpies of Formation of Metal Oxides, Metal Nitrides and of the Oxidation of Metal Nitrides for a Wide Range of Elements

Table S1. Enthalpy changes (ΔH, in kJ/mol)[1] for the formation of metal nitrides (MN), metal oxides (MO) and of the oxidation of MN.

Element	ΔH of MN formation	ΔH of MO formation	ΔH of MN oxidation
Alkaline-earth metals			
Mg	-454.5 (Mg_3N_2)	-601.6 (MgO)	-437.7
Transition metals			
Ti	-374.9 (TiN)	-944.7 (TiO_2)	-656.6
V	-260.9 (VN) -315.6 (V_2N)	-1215(V_2O_3) -1550(V_2O_5)	-1109.9 (V_2O_5) -1316.3 (V_2O_5)
Cr	-144.6 (CrN) -146.5 (Cr_2N)	-1139 (Cr_2O_3)	-871.3 (Cr_2O_3) -1013.9 (Cr_2O_3)
Mn	-92.3 (MnN) -126.0 (Mn_2N) -163.0 (Mn_3N_2)	-519.7 (MnO_2)	-496.9 (MnO_2) -526.1 (MnO_2) -534.8 (MnO_2)
Fe	-60.7 (FeN) -44.4 (Fe_2N)	-824.2 (Fe_2O_3) -1118.4 (Fe_3O_4)	-702.1 (Fe_2O_3) -779.1 (Fe_2O_3)
Co	-6.5 (Co_3N) 4.8 (Co_4N)	-237 (CoO) -891(Co_3O_4)	-918.7 (Co_3O_4) -
Ni	-22.9 (Ni_3N) 48.8 (NiN)	-240 (NiO)	-227.4 (NiO) -
Cu	39.7 (CuN) 101.7 (Cu_2N)	-155.2 (CuO)	- -
Zn	84.3 (ZnN)	-348.0 (ZnO)	-
Y	-385.9 (YN)	-1905 (Y_2O_3)	-1143.9 (Y_2O_3)
Zr	-381.2 (ZrN)	-1100(ZrO_2)	-722.7 (ZrO_2)
Nb	-240.9 (NbN) -288.2 (Nb_2N)	-1920 (Nb_2O_5)	-1567.6 (Nb_2O_5) -1761.0 (Nb_2O_5)
Mo	-105.6 (MoN) -104.4 (Mo_2N)	-745 (MoO_3)	-705.9 (MoO_3) -759.3 (MoO_3)
Ru	15.3 (RuN)	-314 (RuO_2)	-
Rh	64.6 (RhN)	-397 (Rh_2O_3)	-
Pd	27.8 (PdN_2)	-277 (PbO_2)	-
Ag	273.9 (AgN)	-31.1 (Ag_2O)	-
Cd	166.0 (CdN)	-258 (CdO)	-
Hf	-382.6 (HfN) -407.5 (Hf_2N)	-1145 (HfO_2)	-781.0 (HfO_2) -959.8 (HfO_2)
Ta	-262.2 (TaN) -300.1 (Ta_2N)	-2046 (Ta_2O_5)	-1735.9 (Ta_2O_5) -1960.2 (Ta_2O_5)
W	-48.4 (WN) 114.1 (W_2N)	-842 (WO_3)	-832.3 (WO_3) -
Re	-25.9 (ReN)	-1271(Re_2O_7)	-1708.1 (Re_2O_7)
Ir	69.1 (IrN)	-315 (IrO_2)	-
Pt	184.6 (PtN)	-277 (PtO_2)	-
Au	291.4 (AuN)	-11 (Au_2O_3)	-

Metalloids			
B	-282.0 (BN)	-1273(B_2O_3)	-785.8 (B_2O_3)
Si	-892.1 (Si_3N_4)	-911 (SiO_2)	-649.9 (SiO_2)
Ge	-167.3 (Ge_3N_4)	-580 (GeO_2)	-568.5 (GeO_2)
Sb	33.1 (SbN)	-707 (Sb_2O_3)	-
Other Metals			
Al	-318.4 (AlN)	-1675.5 (Al_2O_3)	-1035.9
In	-22.7 (InN)	-925 (In_2O_3)	-918.0 (In_2O_3)
Sn	60.2 (SnN)	-580 (SnO_2)	-
Pb	127.7 (PbN)	-217 (PbO)	-
Bi	95.5 (BiN)	-578 (Bi_2O_3)	-
Lanthanoids			
La	-304.0 (LaN)	-1792 (La_2O_3)	-1261.8 (La_2O_3)
Ce	-336.9 (CeN)	-1087 (CeO_2)	-800.1 (CeO_2)
Pr	-298.3 (PrN)	-3350 (Pr_6O_{11})	-3527.5 (Pr_6O_{11})
Nd	-315.1 (NdN)	-1805 (Nd_2O_3)	-1194.2 (Nd_2O_3)
Pm	-333.3 (PmN)	-1810 (Pm_2O_3)	-1184.0 (Pm_2O_3)
Sm	-341.1 (SmN)	-1817 (Sm_2O_3)	-1181.0 (Sm_2O_3)
Eu	-202.5 (EuN)	-1650 (Eu_2O_3)	-1257.0 (Eu_2O_3)
Gd	-350.3 (GdN)	-1819 (Gd_2O_3)	-1178.7 (Gd_2O_3)
Tb	-381.5 (TbN)	-3150 (Tb_4O_7)	-541.4 (TbO_2)
Dy	-389.9 (DyN)	-1830 (Dy_2O_3)	-1154.5 (Dy_2O_3)
Ho	-397.4 (HoN)	-1840 (Ho_2O_3)	-1151.0 (Ho_2O_3)
Er	-405.2 (ErN)	-1860 (Er_2O_3)	-1146.9 (Er_2O_3)
Yb	-359.8 (YbN)	-1670 (Yb_2O_3)	-1095.0 (Yb_2O_3)
Lu	-427.6 (LuN)	-1905 (Lu_2O_3)	-1134.4 (Lu_2O_3)

References

1. https://next-gen.materialsproject.org/materials